Progress In Electromagnetics Research, Vol. 120, 215–234, 2011

EFFICIENT TIME-DOMAIN ANALYSIS OF WAVEGUIDE DISCONTINUITIES USING HIGHER ORDER FEM IN FREQUENCY DOMAIN

E. M. Klopf [1], S. B. Manić [1], M. M. Ilić [1, 2], and B. M. Notaroš [1, *]

[1]Colorado State University, Department of Electrical and Computer Engineering, Fort Collins, CO 80523-1373, USA

[2]School of Electrical Engineering, University of Belgrade, Belgrade 11120, Serbia

Abstract—A computational technique is presented for efficient and accurate time-domain analysis of multiport waveguide structures with arbitrary metallic and dielectric discontinuities using a higher order finite element method (FEM) in the frequency domain. It is demonstrated that with a highly efficient and appropriately designed frequency-domain FEM solver, it is possible to obtain extremely fast and accurate time-domain solutions of microwave passive structures performing computations in the frequency domain along with the discrete Fourier transform (DFT) and its inverse (IDFT). The technique is a higher order large-domain Galerkin-type FEM for 3-D analysis of waveguide structures with discontinuities implementing curl-conforming hierarchical polynomial vector basis functions in conjunction with Lagrange-type curved hexahedral finite elements and a simple single-mode boundary condition, coupled with standard DFT and IDFT algorithms. The examples demonstrate excellent numerical properties of the technique, which appears to be the first time-from-frequency-domain FEM solver, primarily due to (i) very small total numbers of unknowns in higher order solutions, (ii) great modeling flexibility using large (homogeneous and continuously inhomogeneous) finite elements, and (iii) extremely fast multifrequency FEM analysis (the global FEM matrix is filled only once and then reused for every subsequent frequency point) needed for the inverse Fourier transform.

Received 8 August 2011, Accepted 29 August 2011, Scheduled 6 September 2011

* Corresponding author: Branislav M. Notaroš (notaros@colostate.edu).

1. INTRODUCTION

There is a growing need for electromagnetic modeling and analysis of modern waveguide-based microwave devices, to predict their performance and/or optimize various design parameters prior to costly prototype development [1–6]. The finite element method (FEM), as one of the most powerful and versatile general numerical tools for electromagnetic-field computations [7–10], has been especially effectively used in full-wave three-dimensional (3-D) frequency-domain simulations of a broad range of multiport waveguide structures with arbitrary metallic and dielectric discontinuities, and the FEM is well established as a method of choice for such applications [1, 2]. However, time-domain analysis and characterization of such structures and evaluation of associated transient electromagnetic phenomena are also of great practical importance for a number of well-established and emerging areas of applied electromagnetics, including wideband communication, electromagnetic compatibility, electromagnetic interference, packaging, high-speed microwave electronics, signal integrity, material characterization, and other applications [11–13]. For this purpose, time-domain FEM techniques have recently been developed [8, 13, 14], allowing electromagnetic phenomena to be modeled directly in the time domain. In [8], for instance, the spatially and temporally varying electric field is approximated using interpolatory spatial vector basis functions defined on tetrahedral elements, with time-dependent field-distribution coefficients, which are determined solving the corresponding second-order ordinary differential equation in time by a time-marching procedure. When compared to frequency-domain FEM solutions, time-domain FEM formulations enable effective modeling of time-varying and nonlinear problems and fast broadband simulations (provide broadband information in a single run), at the expense of the additional discretization — in time domain, and the associated numerical complexities, programming and implementation difficulties, and stability and other problems inherent for time-domain computational electromagnetic approaches.

An alternative approach, an indirect time-domain analysis — namely, finding the time-domain response of a microwave passive structure based on the frequency-domain FEM analysis in conjunction with the discrete Fourier transform (DFT) and its inverse (IDFT), seems to have not been exploited, primarily because it requires FEM solutions with many unknowns (unknown field-distribution coefficients to be determined) at many discrete frequency points, which may be very time consuming and computationally prohibitively costly. This paper demonstrates exactly opposite — that with a highly

efficient and appropriately designed frequency-domain FEM technique it is possible to obtain extremely fast and accurate time-domain solutions of microwave passive structures performing computations in the frequency domain along with the DFT/IDFT. The technique is a higher order large-domain Galerkin-type FEM for 3-D analysis of N-port waveguide structures with arbitrary metallic and dielectric discontinuities implementing curl-conforming hierarchical polynomial vector basis functions of arbitrarily high field-approximation orders in conjunction with Lagrange-type curved hexahedral finite elements of arbitrary geometrical orders [2], coupled with standard DFT and IDFT algorithms. The technique allows electrically large elements that are up to about two wavelengths in each dimension (large domains), thus fully exploiting the accuracy, efficiency, and convergence properties of the higher order FEM. It also implements large finite elements with continuous change of medium parameters throughout their volumes, based on Lagrange interpolating schemes for variations of medium parameters [15]. To close the waveguide problem, simple single-mode boundary condition and excitation are introduced across the waveguide ports. This condition appears to be extremely accurate and computationally efficient in the context of the higher order large-domain meshing procedure and FEM solution technique, which enable placing a single large element with a high field-approximation order in the longitudinal direction as a "buffer zone" between each port and the domain with discontinuities, to ensure that the higher modes excited at the discontinuity relax before they reach the port. Finally, the technique is designed, developed, and executed in a form that enables an extremely fast multifrequency analysis of the structure, allowing the global FEM matrix to be filled only once and then reused for every subsequent frequency point, where it should be noted that this is a numerically exact multifrequency analysis, contrary to approximate fast frequency sweep techniques [16]. This is of great importance for the proposed evaluation of the time-domain response of a microwave structure based on the frequency-domain analysis, where we need a large number of frequency samples of the resulting quantities (eg., S-parameters of the structure). To the best of our knowledge, this paper presents the first time-from-frequency-domain FEM solver. Note that a similar approach in the method of moments (MoM) framework (using WIPL-D code) is presented in [17].

Section 2 of the paper presents the main numerical components of the higher order large-domain FEM for transient analysis of microwave passive structures based on frequency-domain computations in conjunction with the DFT and IDFT. In Section 3, the accuracy and efficiency of the new time-from-frequency-domain FEM solver are

evaluated and discussed in three characteristic examples of waveguide structures that include metallic and homogeneous and continuously inhomogeneous dielectric discontinuities. The examples demonstrate excellent numerical properties of the technique based on (i) very small total numbers of unknowns in higher order solutions, (ii) great modeling flexibility using large (homogeneous and inhomogeneous) finite elements, and (iii) extremely fast analysis at multiple frequencies needed for the inverse Fourier transform.

2. THEORY AND IMPLEMENTATION

Consider a 3-D N-port waveguide structure with an arbitrary metallic and/or dielectric discontinuity shown in Fig. 1. In our analysis method, the computational domain is first truncated by introducing fictitious planar surfaces at each of the ports, and thus obtained closed structure is then tessellated using curvilinear geometrical elements. Elements are adopted in the form of Lagrange-type generalized parametric hexahedra of arbitrary geometrical orders K_u, K_v, and K_w (K_u, K_v, $K_w \geq 1$), analytically described as [2, 18]

$$\mathbf{r}(u,v,w) = \sum_{m=0}^{K_u} \sum_{n=0}^{K_v} \sum_{p=0}^{K_w} \mathbf{r}_{mnp} L_m^{K_u}(u) L_n^{K_v}(v) L_p^{K_w}(w), \; -1 \leq u, v, w \leq 1, \quad (1)$$

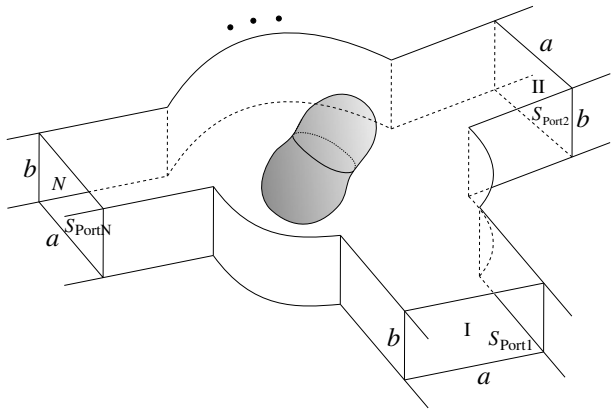

Figure 1. 3-D multiport waveguide structure with an arbitrary discontinuity.

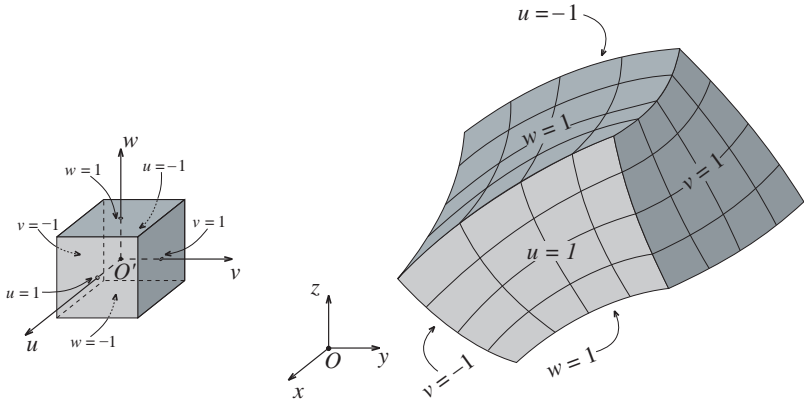

Figure 2. Cube to hexahedron mapping defined by (1) and (2).

with $\mathbf{r}_{mnp} = \mathbf{r}(u_m, v_n, w_p)$ being the position vectors of interpolation nodes and $L_m^{K_u}$ representing Lagrange interpolation polynomials,

$$L_m^{K_u}(u) = \prod_{l=0,\, l\neq m}^{K_u} \frac{u - u_l}{u_m - u_l}, \tag{2}$$

and similarly for $L_n^{K_v}(v)$ and $L_p^{K_w}(w)$. Equations (1) and (2) define a mapping from a cubical parent domain to the generalized hexahedron, as illustrated in Fig. 2. The same Lagrange interpolating scheme is used to describe the continuous variations of both the complex relative permittivity and permeability, ε_r and μ_r, within the hexahedron, as follows [15]:

$$\varepsilon_r(u, v, w) = \sum_{m=0}^{K_u} \sum_{n=0}^{K_v} \sum_{p=0}^{K_w} \varepsilon_{\mathrm{r},mnp}\, L_m^{K_u}(u) L_n^{K_v}(v) L_p^{K_w}(w), \tag{3}$$

where $\varepsilon_{\mathrm{r},mnp} = \varepsilon_r(u_m, v_n, w_p)$ are the relative permittivity values at the points defined by position vectors of spatial interpolation nodes, $\mathbf{r}_{mnp}$, and similarly for μ_r.

The electric fields inside the hexahedra are represented as [2, 18]

$$\begin{aligned}\mathbf{E} = &\sum_{i=0}^{N_u-1} \sum_{j=0}^{N_v} \sum_{k=0}^{N_w} \alpha_{uijk}\ \mathbf{f}_{uijk} + \sum_{i=0}^{N_u} \sum_{j=0}^{N_v-1} \sum_{k=0}^{N_w} \alpha_{vijk}\ \mathbf{f}_{vijk} \\ &+ \sum_{i=0}^{N_u} \sum_{j=0}^{N_v} \sum_{k=0}^{N_w-1} \alpha_{wijk} \mathbf{f}_{wijk},\end{aligned} \tag{4}$$

where $\mathbf{f}$ are curl-conforming hierarchical-type vector basis functions defined as

$$\begin{array}{l} \mathbf{f}_{uijk} = u^i P_j(v) P_k(w) \mathbf{a}'_u, \quad \mathbf{f}_{vijk} = P_i(u) v^j P_k(w) \mathbf{a}'_v, \\ \mathbf{f}_{wijk} = P_i(u) P_j(v) w^k \mathbf{a}'_w. \end{array} \tag{5}$$

The P-functions are simple polynomials representing a higher-order generalization (extension) of one-dimensional rooftop functions,

$$P_i(u) = \begin{cases} 1-u, & i=0 \\ u+1, & i=1 \\ u^i - 1 & i \geq 2, \text{ even} \\ u^i - u & i \geq 3, \text{ odd} \end{cases}, \quad -1 \leq u, v, w \leq 1. \tag{6}$$

Parameters N_u, N_v, and N_w ($N_u, N_v, N_w \geq 1$) are the adopted degrees of the polynomial approximation for fields, and α_{uijk}, α_{vijk}, and α_{wijk} are unknown field-distribution coefficients. The reciprocal unitary vectors $\mathbf{a}'_u$, $\mathbf{a}'_v$, and $\mathbf{a}'_w$ in (5) are obtained as $\mathbf{a}'_u = (\mathbf{a}_v \times \mathbf{a}_w)/J$, $\mathbf{a}'_v = (\mathbf{a}_w \times \mathbf{a}_u)/J$, and $\mathbf{a}'_w = (\mathbf{a}_u \times \mathbf{a}_v)/J$, $J = (\mathbf{a}_u \times \mathbf{a}_v) \cdot \mathbf{a}_w$ being the Jacobian of the covariant transformation and $\mathbf{a}_u = \partial \mathbf{r}/\partial u$, $\mathbf{a}_v = \partial \mathbf{r}/\partial v$, and $\mathbf{a}_w = \partial \mathbf{r}/\partial w$ the unitary vectors, with $\mathbf{r}$ given in (1).

For the general waveguide problem in Fig. 1, we invoke the curl-curl electric-field vector wave equation

$$\nabla \times \mu_r^{-1} \nabla \times \mathbf{E} - k_0^2 \varepsilon_r \mathbf{E} = 0, \tag{7}$$

where $k_0 = 2\pi f \sqrt{\varepsilon_0 \mu_0}$ is the free-space wave number and f is the frequency of the implied time-harmonic variation. A standard Galerkin-type weak form discretization of (7) yields [2, 18]

$$\begin{aligned} &\int_V \mu_r^{-1} \left(\nabla \times \mathbf{f}_{\hat{i}\hat{j}\hat{k}} \right) \cdot (\nabla \times \mathbf{E}\ )\, dV - k_0^2 \int_V \varepsilon_r \mathbf{f}_{\hat{i}\hat{j}\hat{k}} \cdot \mathbf{E} dV \\ &= -\oint_S \mu_r^{-1} \mathbf{f}_{\hat{i}\hat{j}\hat{k}} \cdot \mathbf{n} \times (\nabla \times \mathbf{E})\, dS, \end{aligned} \tag{8}$$

where V is the volume of a generalized hexahedron, $\mathbf{f}_{\hat{i}\hat{j}\hat{k}}$ stands for any of the functions $\mathbf{f}_{u\hat{i}\hat{j}\hat{k}}$, $\mathbf{f}_{v\hat{i}\hat{j}\hat{k}}$ or $\mathbf{f}_{w\hat{i}\hat{j}\hat{k}}$ [testing functions are the same as basis functions in (5)], S is the boundary surface of the hexahedron, and $\mathbf{n}$ is the outward unit normal ($d\mathbf{S} = \mathbf{n} dS$). Due to the continuity of the tangential component of the magnetic field intensity vector, $\mathbf{n} \times \mathbf{H}$, and hence the vector $\mathbf{n} \times (\nabla \times \mathbf{E})$ in (8) across the interface between any two finite elements in the FEM model, the right-hand side term in (8) contains the surface integral over the overall boundary surface of the entire FEM domain, and not over the internal boundary surfaces between the individual hexahedra in the model, which for the waveguide problem in Fig. 1 reduces to the surface integral across the artificially introduced planar surfaces (waveguide ports).

If the waveguide operates in the single-mode regime (which is a standard assumption for practical microwave applications) and the ports are placed far enough from all discontinuities, it can be shown [7] that the boundary condition at the ports can be expressed as

$$\mathbf{n}\times(\nabla\times\mathbf{E})+jk_{z10}\mathbf{n}\times(\mathbf{n}\times\mathbf{E})=\begin{cases}-2jk_{z10}\mathbf{E}^{\text{inc}} & \text{(excitation port)}\\ 0 & \text{(receiving ports)}\end{cases}, \quad (9)$$

where, for a rectangular waveguide, $k_{z10}=\sqrt{k_0^2-(\pi/a)^2}$ is the wave number of the dominant mode (a is the larger dimension of the waveguide cross section), and $\mathbf{E}^{\text{inc}}=E_0\mathbf{e}_{10}e^{-jk_{z10}z}$ is the electric field of the TE_{10} wave, incident on the excitation port. This condition is much easier to implement and faster to compute than alternative multi-mode conditions. However, it has frequently been found to be impractical and computationally costly in traditional small-domain FEM models, due to the fact that placing the ports far from discontinuities (needed to ensure a single-mode simulation) requires a considerable number of additional elements to be employed, which significantly enlarges the computational domain and introduces a large number of new unknowns to be determined. On the other side, this major drawback can be very effectively overcome in the higher order large-domain waveguide modeling, by placing a single large element with a high field-approximation order in the longitudinal direction as a buffer zone between each port and the domain with discontinuities [2]. The sufficient length of the buffer-element allows for the higher modes excited at the discontinuity to relax before they reach the port, while the high-order field expansion in the longitudinal direction ensures the accurate approximation of the fields throughout the element, without introducing an unnecessarily large number of new unknowns.

Substituting the field expansion (4) and the boundary condition (9) into (8) yields the following FEM matrix equation:

$$\big([A]-k_0^2[B]+jk_{z10}[C]\big)\cdot\{\alpha\}=2jk_{z10}\{G\}. \quad (10)$$

Matrix $[A]$ is given by

$$\begin{bmatrix}[UUA] & [UVA] & [UWA]\\ [VUA] & [VVA] & [VWA]\\ [WUA] & [WVA] & [WWA]\end{bmatrix}, \quad (11)$$

and similarly for matrices $[B]$, $[C]$, and $[G]$, where the elements of the

respective submatrices have the form

$$UUA_{\hat{i}\hat{j}\hat{k}ijk} = \int_V \mu_r^{-1} \left(\nabla \times \mathbf{f}_{u\hat{i}\hat{j}\hat{k}}\right) \cdot (\nabla \times \mathbf{f}_{uijk})\, dV, \tag{12}$$

$$UUB_{\hat{i}\hat{j}\hat{k}ijk} = \int_V \varepsilon_r \mathbf{f}_{u\hat{i}\hat{j}\hat{k}} \cdot \mathbf{f}_{uijk} dV, \tag{13}$$

$$UUC_{\hat{i}\hat{j}\hat{k}ijk} = \int_{S_{\text{all ports}}} \mu_r^{-1} \left(\mathbf{n} \times \mathbf{f}_{u\hat{i}\hat{j}\hat{k}}\right) \cdot (\mathbf{n} \times \mathbf{f}_{uijk})\, dS, \tag{14}$$

$$UUG_{\hat{i}\hat{j}\hat{k}ijk} = \int_{S_{\text{excitation port}}} \mu_r^{-1} \left(\mathbf{n} \times \mathbf{f}_{u\hat{i}\hat{j}\hat{k}}\right) \cdot \left(\mathbf{n} \times \mathbf{E}^{\text{inc}}\right) dS, \tag{15}$$

with analogous expressions for the elements corresponding to other combinations of field components. The assembly of a local system of linear equations of the form given by (10) is repeated for each of the elements comprising the mesh, and the global connected system, again of the same form, is solved for the unknown field-distribution coefficients, $\{\alpha\}$. Once they are known, the electric field $\mathbf{E}$ inside the structure in Fig. 1 is computed from (4), and the S-parameters of the structure are obtained as

$$S_{11} = \frac{\int_{S_{\text{Port 1}}} \mathbf{E} \cdot \mathbf{e}_{10} dS}{E_0 \int_{S_{\text{Port 1}}} \mathbf{e}_{10} \cdot \mathbf{e}_{10} dS} - 1, \quad S_{21} = \frac{1}{E_0} \int_{S_{\text{Port 2}}} \mathbf{E} \cdot \mathbf{e}_{10} dS, \tag{16}$$

and so on.

What is very important for finding the time-domain response of multiport waveguide structures based on the frequency-domain analysis, if the materials contained in the structure are dispersionless, integrals appearing in (12)–(15) are frequency independent. Therefore, for a multifrequency analysis of the same structure, which exactly is our case — where we need a large number of frequency samples of the resulting quantities (eg., S-parameters of the structure), these integrals can be calculated only once, conveniently stored, and then recalled during the problem solution for different excitation frequencies, since the only change in the global system is that of the wave number. This procedure significantly reduces the overall computational time for the time response calculation by allowing the global FEM matrix to be filled only once, at the expense of a considerably larger storage space that needs to be allocated, since matrices $[A]$, $[B]$, and $[C]$ have to be stored separately. However, higher order large-domain FEM models of frequently encountered waveguide discontinuity structures require very small numbers of unknowns for high levels of accuracy, which makes them perfect for implementing the described multifrequency solution acceleration procedure within the time-from-frequency-domain FEM solver. Also, it is very important to note that this is a numerically exact

multifrequency analysis, as opposed to approximate fast frequency sweep techniques [16].

To obtain the transient response of the structure in Fig. 1, we excite one of its ports by a causal real signal $E_0(t)$ that is band-limited in the frequency domain. The signal is sampled at N uniformly spaced points over the total time period T, the time step thus amounting to $\Delta t = T/N$, where Δt must satisfy the Nyquist sampling criterion, $\Delta t \leq 1/(2f_{\max})$, i.e., the sampling rate, $f_{\rm s} = 1/\Delta t$, must be at least twice the highest frequency in the spectrum of the signal, $f_{\max}$ [17]. We then compute the frequency-domain response to this excitation, in its discrete (sampled) form, $E_0(t_n)$, as $R(f_k) = S(f_k)E_0(f_k)$, where $E_0(f_k)$ is the discrete Fourier transform (DFT) of $E_0(t_n)$, given by

$$E_0(f_k) = E_0(k) = \sum_{n=0}^{N-1} E_0(t_n) e^{-j\frac{2\pi}{N}nk},\ f_k = k\frac{f_{\rm s}}{N}, k = 0, 1, \ldots, N-1, \quad (17)$$

and $S(f_k)$ is the port-to-port frequency-domain transfer function (namely, an S-parameter) of the structure, which is obtained by the frequency-domain FEM based on (1)–(16), at frequencies f_k ($k = 0, 1, \ldots, N-1$). In fact, since $S(-f) = S^*(f)$, that is, $S(N-k) = S^*(k)$, only $N/2$ frequency points, for $f > 0$, suffice in the FEM analysis. Moreover, as the waveguides in Fig. 1 are assumed to operate in the single-mode (dominant-mode) regime, with buffer elements at the ports included in the FEM region ensuring the relaxation of the higher order modes, we implement a brick-wall band-pass filter to practically use only frequency samples within the dominant frequency range of the waveguide, between the cutoff frequency of the dominant mode and that of the next propagating mode in the structure. Finally, the transient response is evaluated as the inverse discrete Fourier transform (IDFT) of $R(f_k)$, as follows:

$$R(t_n) = R(n) = \frac{1}{N}\sum_{k=0}^{N-1} R(f_k) e^{j\frac{2\pi}{N}nk},\ t_n = n\Delta t,\ n = 0, 1, \ldots, N-1. \quad (18)$$

3. NUMERICAL RESULTS AND DISCUSSION

As the first numerical example, consider a homogeneous lossless dielectric post in a WR-90 rectangular waveguide [13], as shown in Fig. 3(a). The post is illuminated by an incident $\rm TE_{10}$ wave, and we calculate the modal S-parameters using the higher order large-domain FEM. In the analysis, we allow a certain distance between the waveguide ports, at which the S-parameters are calculated, and the discontinuity, as depicted in Fig. 3(b), where the large-domain

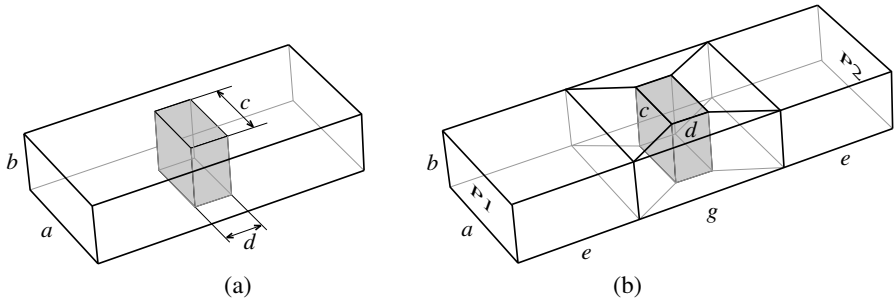

Figure 3. Dielectric ($\varepsilon_r = 8.2$) post discontinuity in a WR-90 waveguide: (a) definition of the structure geometry ($a = 22.86\,\text{mm}$, $b = 10.16\,\text{mm}$, $c = 12\,\text{mm}$, and $d = 6\,\text{mm}$) and (b) higher order large-domain FEM model (mesh) of the structure using generalized hexahedra in Fig. 2 ($e = 45.72\,\text{mm}$ and $g = 24\,\text{mm}$).

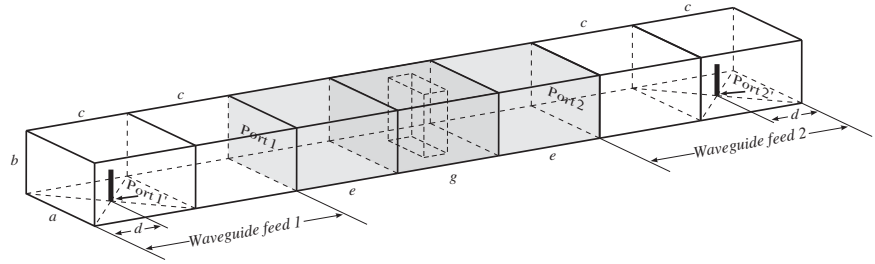

Figure 4. MoM-SIE model of the waveguide structure in Fig. 3: the model includes two waveguide feed sections required for the de-embedding of S-parameters.

FEM model (mesh) is also shown. Note that only seven trilinear ($K_u = K_v = K_w = 1$) hexahedral elements are sufficient to model the structure in this example. The polynomial field-expansion orders (N_u, N_v, and N_w) in the FEM simulation range from 2 to 7 in different elements and different directions.

For the purpose of verification of the numerical results by an alternative computational technique, which is adopted in the form of a higher order MoM within the surface integral equation (SIE) approach [19], a special model is constructed, as shown in Fig. 4, where we first calculate the S-parameters between the two wire probes with point-generators (ports 1' and 2'), and then de-embed the modal S-parameters for the two-port section between ports 1 and 2 [20]. In addition, the higher order FEM results are verified against the results obtained using the commercial FEM software HFSS.

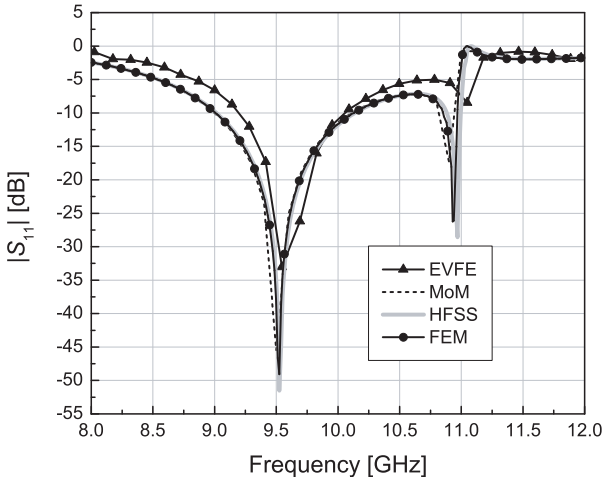

Figure 5. Frequency-domain results for the S_{11}-parameter of the dielectrically loaded waveguide in Fig. 3.

The magnitude of the computed S_{11}-parameter of the dielectrically loaded waveguide structure in Fig. 3 is plotted in Fig. 5. The results obtained by the higher order FEM are compared to the envelope-finite element (EVFE) results from [13], to the results obtained by the MoM-SIE technique [19], and to the HFSS results, and a very good agreement between the four sets of results is observed. Note that the results obtained by the higher order FEM and MoM and by HFSS (all directly in the frequency domain) agree extremely well, while the EVFE results (extracted from a time-domain solution) are slightly different.

In terms of the computational efficiency, the computational time required for the higher order FEM simulation (with 7 generalized hexahedral elements and 1012 unknowns) on a 3 GHz CPU PC computer (Intel® Core i5 760 at 3 GHz) is 2.9 seconds for matrix filling (only once) and only 0.03 seconds for the solution for S-parameters per every frequency point, so that the total simulation time (at 300 frequencies) is 11.9 seconds. The total simulation time using HFSS (with 3574 tetrahedral finite elements) is 332 seconds on the same computer. Hence, the higher order FEM is 28 times faster than HFSS in this case. We consider this higher order FEM simulation to be extremely fast and suitable for large frequency sweeps necessary for the generation of transient responses.

We next calculate the transient response of the waveguide structure in Fig. 3 exciting it by a modulated Gaussian pulse expressed

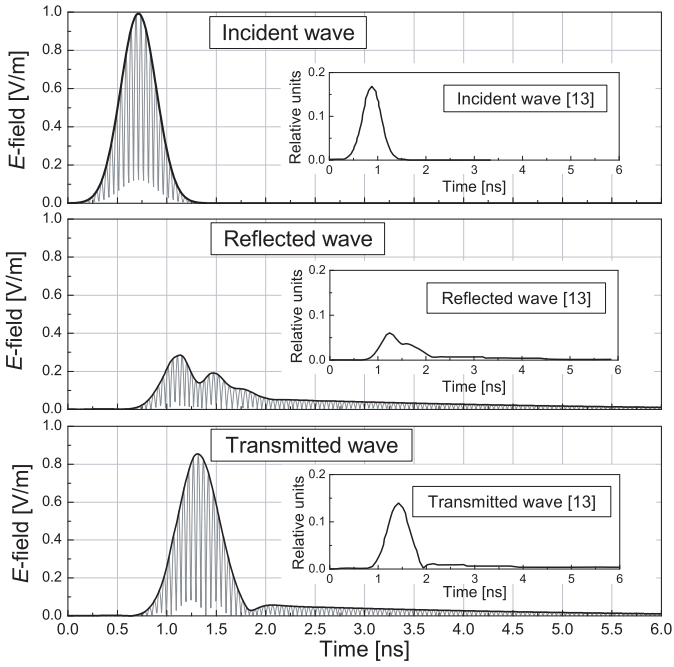

Figure 6. Transient waveforms of incident, reflected, and transmitted waves for the structure in Fig. 3 and excitation in (19) obtained by the FEM-DFT/IDFT technique (note that rectified modulated signals are shown within the envelopes); EVFE results from [13] are shown in figure insets.

as [13]

$$E_0(t) = e^{-4\left(\frac{t-t_0}{T}\right)^2} \sin\left[2\pi f_c(t-t_0)\right] \text{ V/m}, \tag{19}$$

where the carrier frequency is $f_c = 10\,\text{GHz}$, half bandwidth is $\Delta f = 2.5\,\text{GHz}$, $T = 4/(\pi\Delta f)$, and $t_0 = 1.4T$. The parameters of DFT/IDFT calculations are as follows: the sampling frequency is $f_s = 200\,\text{GHz}$ (time step is $\Delta t = 1/f_s = 5\,\text{ps}$) and the number of samples is $N = 2048$; in fact, we compute responses only at frequency points within the dominant frequency range of the waveguide. The obtained transient waveforms, shown in Fig. 6, are in a good agreement with EVFE responses from [13] (shown in figure insets), having in mind that the two sets of results are obtained with different waveguide excitations — current probes in [13] (with no details provided), as opposed to modal excitations in this present work, as well as that no details are provided in [13] about the actual locations of reference planes with respect to which the responses are given.

Based on a close analysis of the reflected wave in Fig. 6, we realize that the two peaks occurring at $t_{\text{refl1}} \approx 1.135\,\text{ns}$ and $t_{\text{refl2}} \approx 1.5\,\text{ns}$ correspond to the waves reflected from the front and rear sides of the dielectric post, respectively. Note also that, although the nonloaded waveguide sections in front of and behind the post are equally long, the maximum of the transmitted wave, in Fig. 6, arrives at the second port at $t_{\text{trans}} \approx 1.32\,\text{ns}$, which is in between t_{refl1} and t_{refl2}. This can be attributed to the fact that the transmitted wave travels a slightly shorter distance (from port 1 to port 2) than the wave reflected from the rear side of the post (from port 1 to the rear side and back to port 1). Additionally, the wave reflected from the front side of the post travels only in air (hence, it is the fastest), the wave reflected from the rear side makes a round trip inside the dielectric post (which slows it down considerably), and the transmitted wave travels through the dielectric only in one direction (and thus its average velocity is between those of the other two waves).

As the second example, consider a WR-62 waveguide with two crossed metallic cylindrical posts, the higher order FEM model of which is shown in Fig. 7. The higher order FEM solution in the frequency domain is compared with numerical results by HFSS and with measured data [21], and we observe in Fig. 8 a very good agreement of the three sets of results for the S_{11} of the structure. For the higher order FEM (with ten curved and straight generalized hexahedral elements, field-expansion orders ranging from 2 to 5, and 1184 unknowns), matrix filling time is 9 seconds and solving time is 0.05 seconds per frequency, which results in a total computational time of 24 seconds for the 12–18 GHz discrete frequency sweep in 300 points (on a 3 GHz CPU PC computer). The HFSS FEM solution (with 3157 tetrahedral elements) takes 314 seconds of computational time for the same frequency sweep on the same computer, which makes the higher order solution 13 times faster.

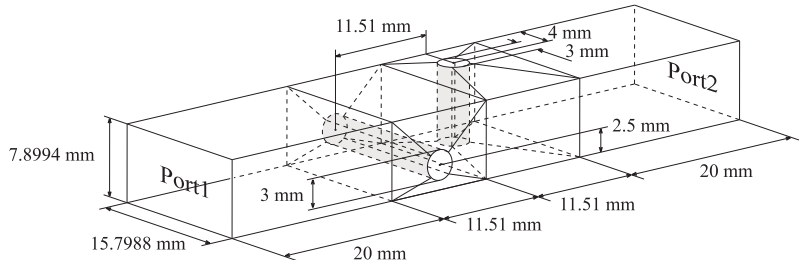

Figure 7. Ten-element higher order FEM model of a WR-62 waveguide with two crossed metallic cylindrical posts.

The transient response of the structure in Fig. 7 computed using the FEM-DFT/IDFT simulation is shown in Fig. 9, where, for the excitation in (19), $f_c = 14\,\text{GHz}$ and $\Delta f = 3\,\text{GHz}$, the sampling frequency amounts to $f_s = 280\,\text{GHz}$ ($\Delta t \approx 3.57\,\text{ps}$), and the numbers of time and frequency samples are the same as in Fig. 6.

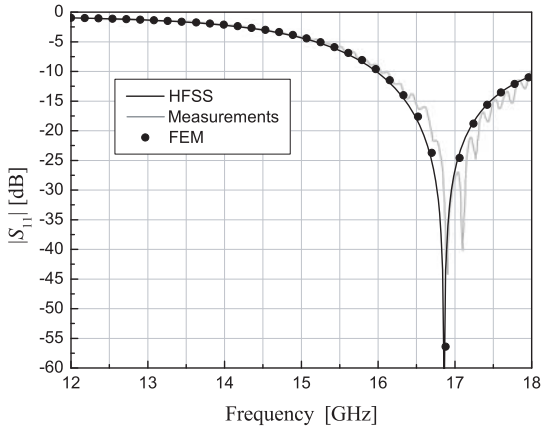

Figure 8. S_{11}-parameter of the waveguide structure in Fig. 7; measured data are from [21].

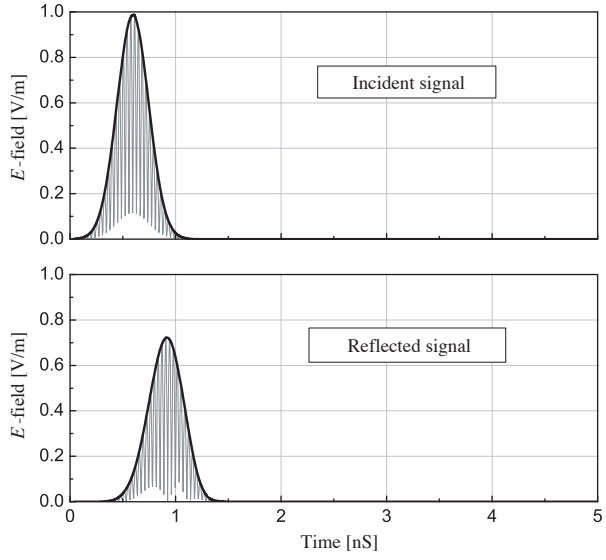

Figure 9. Transient response of the waveguide structure in Fig. 7 obtained by the FEM-DFT/IDFT technique.

The last example is a WR-15 waveguide loaded with a continuously inhomogeneous dielectric slab where $\varepsilon_r(u) = 9 - 8u^2$, $-1 < u < 1$ and $u = 2z/c - 1$, as portrayed in Fig. 10, where two simple large-domain FEM models are shown as well. The continuously inhomogeneous section is (i) modeled by a single continuously inhomogeneous finite element and (ii) approximated by a series of piecewise homogeneous dielectric layers, respectively. When the piecewise homogeneous approximation of the dielectric profile is implemented, the original slab is subdivided into N_{layers} equally thick layers with individual permittivities calculated as an average permittivity of the original profile in the corresponding coordinate range, i.e.,

$$\varepsilon_{\text{r}i} = \frac{1}{\Delta z}\int_{z_i}^{z_i+\Delta z} \varepsilon_r(z)dz\,, \quad \Delta z = \frac{c}{N_{\text{layers}}}\,, \quad z_i = (i-1)\Delta z \tag{20}$$

($i = 1, 2, \ldots, N_{\text{layers}}$). Such piecewise constant permittivities for $N_{\text{layers}} = 3$, 5, and 7, respectively, are given in Table 1.

Results of the frequency-domain analysis of the waveguide structure in Fig. 10 are shown in Fig. 11. In the graphs, the higher order FEM solution with the continuously inhomogeneous model is compared to higher order FEM simulations of piecewise homogeneous models with $N_{\text{layers}} = 3$ and 7, respectively, to higher order MoM-SIE [19] results for the $N_{\text{layers}} = 7$ approximate model (excitation/reception by wire probes and S-parameter de-embedding are done as in Fig. 4), and to the HFSS solution for the $N_{\text{layers}} = 7$ model. It is clearly seen that the model with three layers provides a poor approximation of the continuous permittivity profile of the slab, yielding very inaccurate S_{11} in both magnitude and phase (both equally important for the accurate calculation of transient responses), and that seven (and more) layers are necessary to obtain a fairly good approximation of the profile resulting in a rather accurate S-parameter characterization. We also observe an almost exact match of the higher order FEM, MoM, and HFSS solutions for the same $N_{\text{layers}} = 7$ model.

Table 1. Dielectric permittivities constituting three piecewise homogeneous layered approximations of the continuously inhomogeneous dielectric slab in Fig. 10 obtained using (20).

N_{layers}	$\varepsilon_{\text{r}1}$	$\varepsilon_{\text{r}2}$	$\varepsilon_{\text{r}3}$	$\varepsilon_{\text{r}4}$	$\varepsilon_{\text{r}5}$	$\varepsilon_{\text{r}6}$	$\varepsilon_{\text{r}7}$
3	5.14815	8.7037	5.14815				
5	3.77333	7.61333	8.89333	7.61333	3.77333		
7	3.06803	6.33333	8.29252	8.94558	8.29252	6.33333	3.06803

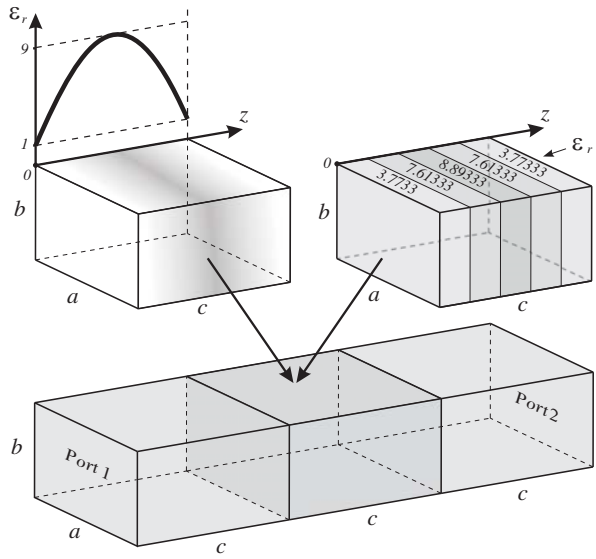

Figure 10. Three-element higher order large-domain FEM model of a WR-15 waveguide ($a = 3.76\,\text{mm}$, $b = 1.88\,\text{mm}$, and $c = 2.5\,\text{mm}$) with a continuously inhomogeneous lossless dielectric load (central element) whose permittivity varies quadratically in the longitudinal direction; five-layer ($N_{\text{layers}} = 5$) model of the load with piecewise constant approximation of the permittivity profile, according to (20), is also shown.

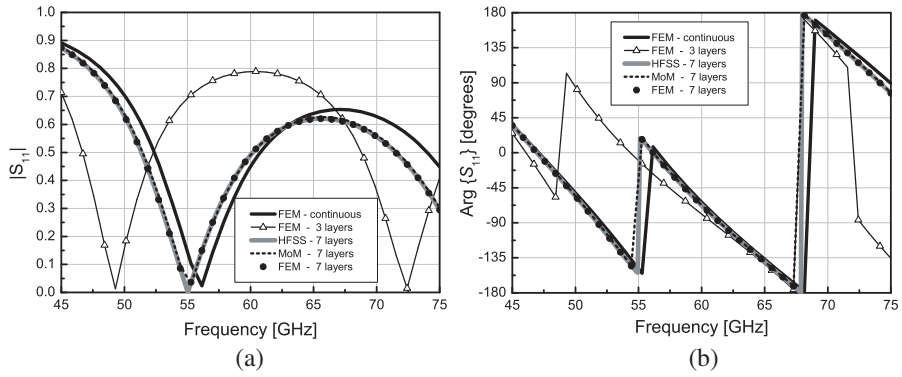

Figure 11. Magnitude and phase (argument) of the S_{11}-parameter of the waveguide structure with a continuously inhomogeneous dielectric load in Fig. 10.

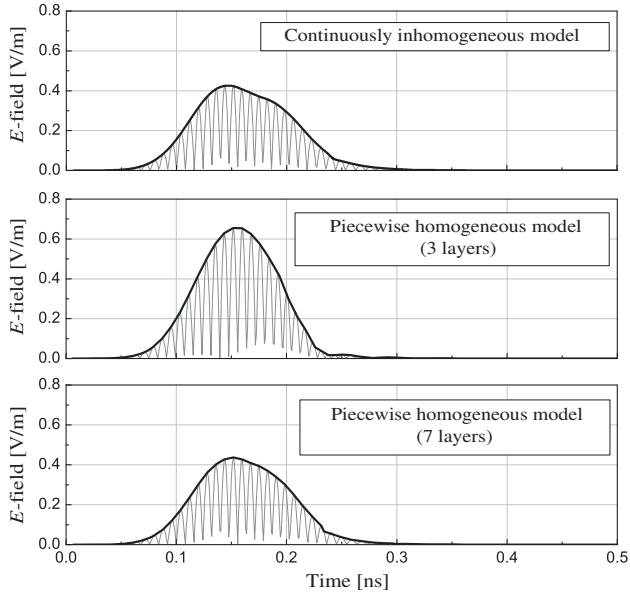

Figure 12. Transient response — reflected wave — of the structure in Fig. 10 computed using the FEM-DFT/IDFT technique applied to models with the continuous permittivity profile, with the 3-layer approximation of the load (see Table 1), and with the 7-layer approximation, respectively.

The continuously inhomogeneous higher order FEM model [with only 3 hexahedral finite elements (one inhomogeneous dielectric element and two buffer elements) and only 205 unknowns] takes a total of only 3 seconds of computational time for 300 frequencies (matrix filling time is 1.02 seconds, while solving time per frequency is undetectable) on a 3 GHz CPU PC. With HFSS (3674 tetrahedral finite elements), the total computational time (for 300 frequencies) amounts to 398 seconds on the same computer, so the higher order FEM comes out to be 132.7 times faster than the HFSS solution.

For the transient analysis of the structure in Fig. 10, we employ the excitation in (19) with $f_c = 62\,\text{GHz}$ and $\Delta f = 15\,\text{GHz}$. The sampling frequency is now $f_s = 1240\,\text{GHz}$ ($\Delta t \approx 0.8\,\text{ps}$), whereas the numbers of time and frequency samples are the same as in Fig. 6. The results of the FEM-DFT/IDFT computation are shown in Fig. 12, where we conclude, as expected based on the frequency-domain results in Fig. 11, that the transient response of the $N_{\text{layers}} = 3$ approximate model is significantly less accurate than that with $N_{\text{layers}} = 7$, as compared to the FEM model with the inhomogeneous profile modeled exactly.

4. CONCLUSIONS

This paper has presented a computational technique for efficient and accurate time-domain analysis of multiport waveguide structures with arbitrary metallic and dielectric discontinuities using a higher order FEM in the frequency domain. It has demonstrated that with a highly efficient and appropriately designed frequency-domain FEM solver, it is possible to obtain extremely fast and accurate time-domain solutions of microwave passive structures by performing computations in the frequency domain along with the discrete Fourier transform and its inverse. The technique is a higher order large-domain Galerkin-type FEM for 3-D analysis of waveguide structures with discontinuities implementing curl-conforming hierarchical polynomial vector basis functions in conjunction with Lagrange-type curved hexahedral finite elements, coupled with standard DFT and IDFT algorithms. To close the waveguide problem, a simple single-mode boundary condition has been introduced across the waveguide ports, with a large buffer finite element at each port to ensure relaxation of higher modes. The technique enables an extremely fast multifrequency analysis of a microwave structure, allowing the global FEM matrix to be filled only once and then reused for every subsequent frequency point, which is of great importance for the evaluation of the time-domain response of the structure based on the frequency-domain analysis. Numerical examples of waveguide structures that include homogeneous and continuously inhomogeneous dielectric discontinuities, as well as metallic ones, have validated and verified the accuracy and efficiency of the presented technique, which appears to be the first time-from-frequency-domain FEM solver. The examples have demonstrated excellent numerical properties of the technique primarily due to (i) very small total numbers of unknowns in higher order solutions, (ii) great modeling flexibility using large (homogeneous and inhomogeneous) finite elements, and (iii) extremely fast FEM solutions at multiple frequencies needed for the inverse Fourier transform.

ACKNOWLEDGMENT

This work was supported by the National Science Foundation under grants ECCS-0650719 and ECCS-1002385 and by the Serbian Ministry of Science and Technological Development under grant TR-32005. The authors thank Dr. Dragan Olćan for invaluable discussions.

REFERENCES

1. Rubio, J., J. Arroyo, and J. Zapata, "Analysis of passive microwave circuits by using a hybrid 2-D and 3-D finite-element mode-matching method," *IEEE Transactions on Microwave Theory and Techniques*, Vol. 47, No. 9, 1746–1749, September 1999.
2. Ilić, M. M., A. Ž. Ilić, and B. M. Notaroš, "Higher order large-domain FEM modeling of 3-D multiport waveguide structures with arbitrary discontinuities," *IEEE Transactions on Microwave Theory and Techniques*, Vol. 52, No. 6, 1608–1614, June 2004.
3. El Sabbagh, M. and K. Zaki, "Modeling of rectangular waveguide junctions containing cylindrical posts," *Progress In Electromagnetics Research*, Vol. 33, 299–331, 2001.
4. Booty, M. R. and G. A. Kriegsmann, "Reflection and transmission from a thin inhomogeneous cylinder in a rectangular TE_{10} waveguide," *Progress In Electromagnetics Research*, Vol. 47, 263–296, 2004.
5. Khalaj-Amirhosseini, M., "Microwave filters using waveguides filled by multi-layer dielectric," *Progress In Electromagnetics Research*, Vol. 66, 105–110, 2006.
6. Sjöberg, D., "Determination of propagation constants and material data from waveguide measurements," *Progress In Electromagnetics Research B*, Vol. 12, 163–182, 2009.
7. Jin, J. M., *The Finite Element Method in Electromagnetics*, 2nd Edition, John Wiley & Sons, New York, 2002.
8. Jin, J. M. and D. J. Riley, *Finite Element Analysis of Antennas and Arrays*, John Wiley & Sons, New York, 2008.
9. Notaroš, B. M., "Higher order frequency-domain computational electromagnetics," Special Issue on Large and Multiscale Computational Electromagnetics, *IEEE Transactions on Antennas and Propagation*, Vol. 56, No. 8, 2251–2276, August 2008.
10. Rui, X., J. Hu, and Q. H. Liu, "Higher order finite element method for inhomogeneous axisymmetric resonators," *Progress In Electromagnetics Research B*, Vol. 21, 189–201, 2010.
11. Kristensson, G., "Transient electromagnetic wave propagation in waveguides," *Journal of Electromagnetic Waves and Applications*, Vol. 9, No. 5–6, 645–671, 1995.
12. Rothwell, E. J., A. K. Temme, and B. R. Crowgey, "Pulse reflection from a dielectric discontinuity in a rectangular waveguide," *Progress In Electromagnetics Research*, Vol. 97, 11–25, 2009.

13. Tsai, H. P., Y. Wang, and T. Itoh, "Efficient analysis of microwave passive structures using 3-D envelope-finite element (EVFE)," *IEEE Transactions on Microwave Theory and Techniques*, Vol. 50, No. 12, 2721–2727, December 2002.
14. Faghihi, F. and H. Heydari, "A combination of time domain finite element-boundary integral with time domain physical optics for calculation of electromagnetic scattering of 3-D structures," *Progress In Electromagnetics Research*, Vol. 79, 463–474, 2008.
15. Ilić, M. M., A. Ž. Ilić, and B. M. Notaroš, "Continuously inhomogeneous higher order finite elements for 3-D electromagnetic analysis," *IEEE Transactions on Antennas and Propagations*, Vol. 57, No. 9, 2798–2803, September 2009.
16. De la Rubia, V., U. Razafison, and Y. Maday, "Reliable fast frequency sweep for microwave devices via the reduced-basis method," *IEEE Transactions on Microwave Theory and Techniques*, Vol. 57, No. 12, 2923–2937, December 2009.
17. Olćan, D. I., M. M. Nikolić, B. M. Kolundžija, and A. R. Djordjević, "Time-domain response of 3-D structures calculated using WIPL-D," *Proceedings of the 2007 Annual Review of Progress in Applied Computational Electromagnetics*, 525–531, Verona, Italy, March 2007.
18. Ilić, M. M. and B. M. Notaroš, "Higher order hierarchical curved hexahedral vector finite elements for electromagnetic modeling," *IEEE Transactions on Microwave Theory and Techniques*, Vol. 51, No. 3, 1026–1033, March 2003.
19. Djordjević, M. and B. M. Notaroš, "Double higher order method of moments for surface integral equation modeling of metallic and dielectric antennas and scatterers," *IEEE Transactions on Antennas and Propagation*, Vol. 52, No. 8, 2118–2129, August 2004.
20. Kolundžija, B., B. Janić, and M. Rakić, "Novel technique for deembeding S-parameters in electromagnetic modeling of arbitrary circuits," *IEEE APS International Symposium Digest*, 2784–2787, Monterey, CA, USA, June 2004.
21. Bunger, R. and F. Arndt, "Moment-method analysis of arbitrary 3-D metallic N-port waveguide structures," *IEEE Transactions on Microwave Theory and Techniques*, Vol. 48, No. 4, 531–537, April 2000.